Title

Nuclear respiratory factor 1 promotes spheroid survival and mesenchymal transition in mammary epithelial cells

Journal

Oncogene, 37(47)

ISSN

0950-9232

Authors

Zhou, Yuanshuai
Xu, Zhongjuan
Quan, Daniel
et al.

Publication Date

2018-11-01

DOI

10.1038/s41388-018-0349-2

Peer reviewed

HHS Public Access

Author manuscript

Oncogene. Author manuscript; available in PMC 2019 March 15.

Published in final edited form as:

Oncogene. 2018 November ; 37(47): 6152–6165. doi:10.1038/s41388-018-0349-2.

Nuclear respiratory factor 1 promotes spheroid survival and mesenchymal transition in mammary epithelial cells

Yuanshuai Zhou[1,2], **Zhongjuan Xu**[1], **Daniel Quan**[3], **Fan Zhang**[4], **Hai Zhang**[1], **Tongqian Xiao**[1,2], **Shulan Hou**[1], **Hong Qiao**[4], **Olivier Harismendy**[3], **Jean Y. J. Wang**[3], and **uangli Suo**[1]

[1]CAS Key Laboratory of Nano-Bio Interface, Suzhou Institute of Nano-Tech and Nano-Bionics, Chinese Academy of Sciences, Jiangsu 215123, China

[2]University of Chinese Academy of Sciences, Beijing 100049, China

[3]Division of Hematology/Oncology, Department of Medicine, Moores Cancer Center, University of California, San Diego, School of Medicine, La Jolla, CA 92093-0820, USA

[4]Department of Molecular Biosciences, The University of Texas at Austin, Austin, TX 78712, USA

Abstract

Epithelial cells aggregate into spheroids when deprived of matrix, and the proclivity for spheroid formation and survival is a hallmark of normal and tumorigenic mammary stem cells. We show here that Nuclear Respiratory Factor 1 (NRF1) is a spheroid promoter by in silico identification of this transcription factor as highly connected to top shRNA-hits deduced from re-iterative selections for shRNAs enriched in MCF10A spheroids. NRF1-promoted spheroid survival is linked to its stimulation of mitochondrial OXPHOS, cell migration, invasion, and mesenchymal transition. Conversely, NRF1 knockdown in breast cancer MDA-MB-231 cells reduced spheroids, migration, invasion, and mesenchymal marker expression. NRF1 knockdown also reduced tumor burden in mammary fat pads and lungs of orthotopic- or tail veintransplanted mice. With the Luminal A subtype of breast cancer, higher NRF1 expression is associated with lower survival. These results show that NRF1, an activator of mitochondrial metabolism, supports mammary spheroid survival and tumor development.

Introduction

Polarized epithelial cells form basal and lateral adhesions with the basement membrane and neighboring cells, respectively. The basal adhesion requires integrin receptors interacting with the extracellular matrix (ECM) proteins, whereas the lateral cell–cell adhesions are stabilized through the formation of adherence junctions and tight junctions. Survival of polarized epithelial cells is critically dependent on these adhesive interactions as detachment

Guangli Suo glsuo2013@sinano.ac.cn. These authors contributed equally: Yuanshuai Zhou, Zhongjuan Xu. These authors jointly supervised this work: Jean Y. J. Wang, Guangli Suo.

Compliance with ethical standards

Conflict of interest The authors declare that they have no conflict of interest.

Electronic supplementary material The online version of this article (https://doi.org/10.1038/s41388–018-0349–2) contains supplementary material, which is available to authorized users.

from the ECM can activate intrinsic apoptosis, namely anoikis, in epithelial cells [1]. Besides intrinsic apoptosis, ECM deprivationinduced cell death also involves extrinsic apoptosis induced by TRAIL [2] and autophagy [3]. Even when apoptosis is blocked by the overproduction of BCL2 in MCF10A mammary epithelial cells, ECM deprivation still causes viability loss as a result of disruption in glucose utilization, ATP production, and redox homeostasis [4]. When plated in suspension culture, detached MCF10A cells can escape apoptosis by aggregating into multicellular mammary spheroids [5]. However, these aggregated spheroid cells still lose viability with time in detached cultures most likely because of the disruption in energy and redox metabolism [4, 6]. Neoplastic transformation of epithelial cells is associated with the loss of anoikis and the gain of ECMindependent survival [7]. The proclivity for growth and survival in detached cultures as spheres or spheroids has widely been considered a hallmark of epithelial cancer stem cells [8–11]. This gain of resistance to ECM-deprivation also contributes to survival of circulating tumor cells and can therefore promote metastasis [12].

The ERBB2 oncogene of breast cancer has been shown to promote ECM-independent glucose utilization and thus stimulating the survival of matrix-deprived MCF10A cells [4, 13]. On the other hand, there have not been any studies on genes that suppress the survival of matrix-deprived MCF10A cells. To find genes that are required for matrixdeprived MCF10A cells to lose viability, we took a nonbiased approach by screening a genome-wide shRNA library for shRNA sequences that were enriched in pools of cells that survived repeated rounds of selection as spheroids in detached cultures. Among the shRNAs significantly enriched in the surviving cell pools, we found that the top two shRNAs are predicted to target genes that encode mitochondrial proteins. Because metabolic fitness underlined the ERBB2-induced survival of MCF10A spheroids [4], and because an in silico analysis of the ENCODE database found nuclear respiratory factor-1 (NRF1) to be a hub with significant connectivity to the top shRNA-hits, we investigated the role of NRF1 in mammary spheroid survival.

NRF1 encodes a transcription factor (TF) that regulates the expression of nuclear genes required for mitochondrial metabolism, including respiration, heme biosynthesis, and mitochondrial DNA transcription and replication [14–16]. It was also reported to be an estrogen response gene in MCF7 breast cancer cells [17]. Emerging evidence has suggested that a critical subpopulation of cancer cells responsible for tumor maintenance, metastasis, and stress resistance tend to rely more on mitochondrial respiration than glycolytic catabolism for ATP generation [18–20]. We showed here that NRF1 interacts with the promoter regions of several shRNA-hits from our screen and that NRF1 reduced the expression of those genes, which our screen selected as potential suppressors of spheroid viability. Furthermore, we found that NRF1 not only stimulated spheroid survival but also activated mesenchymal traits in the non-tumorigenic MCF10A cells and in breast cancer cells. We also found an association of higher NRF1 expression with poorer survival among the Luminal A subtype of breast cancer.

Results

Identification of shRNAs enriched in MCF10A cells surviving repeated rounds of suspension culture as spheroids

In suspension culture on low-attachment plates, MCF10A mammary epithelial cells die rapidly as single cells or aggregate into spheroids to escape apoptosis. Small aggregates of spheroids could be detected in suspension culture at 24 h after detachment and they fused into larger aggregates with time. We found that the majority of spheroid cells retained proliferative potential for up to 48 h in suspension culture. However, by 60 h, the cloning efficiency of spheroid cells was reduced to 0.05% when they were dissociated and replated on attachment plates (Fig. 1b). By comparison, the cloning efficiency of MCF10A cells after 60 h of attached culturing was 200-fold higher, at around 10% (Fig. 1b). Staining of spheroids with Sytox Green showed that only a small fraction of cells in each MCF10A spheroid was dead at 72 h (Supplementary Figure 1c). These results suggested that viability loss in spheroids was caused by a combination of physical death and metabolic decline. This time-dependent loss of viability was not observed with spheroids formed by the MCF7 breast cancer cells (Fig. 1b, c), consistent with previous findings that breast cancer cells can maintain metabolic fitness despite matrix deprivation [6].

To identify genes that suppress spheroid survival in nontumorigenic mammary epithelial cells, we transduced MCF10A cells with a genome-wide shRNA library through lentiviral infection (Fig. 1a). Following puromycin selection, we extracted genomic DNA from half of the librarytransduced population to determine the shRNA sequences in the starting pool. We subjected the other half of the library-transduced population to several rounds of selection for survival in spheroid culture (Fig. 1a). In each round of selection, detached cells were allowed to form spheroids on poly-HEMA coated plates for 60 h and then replated on attached plates for expansion to collect sufficient cells for the next round of selection (Fig. 1a). MCF10A pool infected with empty lentiviral vector (vector-infected) did not acquire higher survival efficiency after two rounds of selection (Fig. 1c). Due to the long expansion time of vector-infected MCF10A pool, we terminated this control culture after 2 rounds. The survival fraction of shRNAlibrary-transduced pools, however, increased with each round of selection in two independent experiments (Pool-a and Pool-b), reaching a plateau of ~50% after five to six rounds (Fig. 1c). To assess how disabling apoptosis might affect spheroid survival, we stably knocked-down BAX in MCF10A cells (Supplementary Figure 1d) and then measured the survival fraction of BAX-knockdown (BAXkd) MCF10A cells after each of 6 rounds of selection. We found that BAX-kd also increased the survival fraction but reached a plateau of ~5% after 3 rounds (Fig. 1c). Thus, apoptosis reduction contributed to spheroid survival but not to the extent achieved by other shRNAs in the library.

To identify shRNA sequences that were enriched in spheroids after 7 rounds of selection, we amplified the integrated shRNA cassettes in genomic DNA from the starting and the selected pools of MCF10A cells, and applied NextGen sequencing to collect read-counts of the amplicon sequences (Fig. 1a, Supplementary Figure 1a and b). From the starting cell pool, we found 33,682 unique shRNA-sequences mapping to 11,523 unique human genes after filtering and aligning to the human genome assembly (Hg19) (Supplementary Table 1). In

the 7-round selected spheroid cell pool, we found 677 unique shRNA-sequences mapping to 587 human genes. The shRNAs were ranked by significance of enrichment in the 7-round selected cell pool, and the top 8 shRNA sequences are predicted to target *CCDC90B, IDH3B, IL13RA1, AJAP1, LITAF, PUDP, LRP12,* and *GEMIN2* (Fig. 1d).

To validate the pool screen result, we expressed the most highly enriched shRNA, which is complementary to the 3′untranslated region of *CCDC90B*, by using the pLKO lentiviral vector (Supplementary Figure 2a and b). CCDC90B is a paralogue of CCDC90A, an evolutionarily conserved mitochondrial protein that has been implicated in the regulation of mitochondrial calcium uniporter and respiratory Complex IV. [21, 22]. We found that de novo expression of this shRNA in MCF10A cells down-regulated CCDC90B and leading to larger sizes and higher ATP levels of spheroids than the pLKO-vector cells (vector-KD) in suspension culture (Supplementary Figure 2c-g). However, de novo expression of this CCDC90B-shRNA caused only a 2–3-fold increase in the survival fraction of spheroid cells relative to pLKO-vector control, but not to the 50% level observed with the 7-round selected pool. Because spheroids were formed by cell aggregation rather than clonal outgrowth during the 60 h of selection in suspension culture, and because de novo expression of the most highly enriched shRNA (CCDC90B) was not sufficient to raise survival to the level of the selected pool, we considered the possibility that multiple different shRNA-expressing cells in the 7-round selected pool might have each gained some survival advantage and it was their aggregation into spheroids that resulted in ~50% survival. We therefore reasoned that by exploring the connectivity among the top shRNA-hits, we might gain insights into other, more central, regulators of spheroid survival. Because cell fate decisions such as death vs. survival are generally controlled by master TFs, we focused the in silico analysis on TFs that may connect the predicted shRNA-hits.

Informatics identification of transcription factors targeting shRNA-hits

We searched the ENCODE ChIP-Seq database for TFs with binding sites in the promoter regions (2-kb upstream of transcription start site) of the top shRNA-hits. In ENCODE, we found 24,103 genes (N) with ChIP-seq peaks in the 2-kb upstream regions. The top 8 shRNA-hits (n) (Fig. 1e) are among the 24,103 genes, and ENCODE showed 136 TFs in the 2-kb upstream regions of those 8 genes. Given that each TF can target numerous genes and each gene is regulated by many TFs, we performed Fisher's exact test (see Materials and methods for formula) to define hub TFs as those with a significant preference for the top shRNA-hits (p value ≤ 0.05). From the 136 TFs, we identified 17 such "hubs" (Fig. 1f). These hubs included master regulators such as *MYC* and *E2F* with well-established roles in the regulation of cell growth and death. Using *MYC* as an example, the ENCODE database showed 11,311 genes (M) to bind MYC in the promoter regions. Among the 8 top shRNA-hits, the ENCODE database showed 7 (m) to contain *MYC* binding sites. The Fisher's exact test calculated the p value for *MYC* connectivity to the top shRNA-hits to be 0.0236. For Nuclear Respiratory Factor 1 (NRF1), with $M = 5469$ and $m = 5$, the Fisher's exact test calculated the p value to be 0.018 (Fig. 1f). Because the top two shRNA hits (*CCDC90B* and *IDH3B*) encode mitochondrial proteins, and because NRF1 is a master regulator of mitochondrial biogenesis and energy metabolism, we focused the subsequent validation experiments on this TF. We experimentally confirmed the ENCODE data by showing that

NRF1 interacted with the promoter regions of *CCDC90B*, *IDH3B*, *LRP12*, and *PUDP* in MCF10A cells overexpressing NRF1 (10A-NRF1-OE cells) (Supplementary Figure 3a and b). We also showed that NRF1 reduced the levels of *CCDC90B*, *IDH3B*, *LRP12*, and *PUDP RNA* (Supplementary Figure 3c). The result that NRF1 overexpression had a negative effect on the RNA levels showed that NRF1 had a similar effect as the shRNAs on the expression of these shRNA-hits. In other words, NRF1 overexpression could reduce the expression of the putative "spheroid suppressor genes" deduced from our screen.

NRF1 stimulates spheroid formation and survival

To examine the effects of NRF1 on spheroids in nontumorigenic mammary epithelial cells and breast cancer cells, we stably expressed NRF1-cDNA in MCF10A cells (10A-NRF1-OE) and NRF1-shRNA in MDA-MB-231 cells (231-NRF1-KD) (Fig. 2a). We found that overexpression of NRF1 stimulated MCF10A spheroid formation both in size (Fig. 2b) and number (Fig. 2c), and increased the survival of spheroid cells (Fig. 2d) in suspension cultures. Overexpression of NRF1 also reduced anoikis (Fig. 2h, i), abrogated the hollow lumen and stimulated lumen-less aggregates in Matrigel cultures (Fig. 2l, m). In breast cancer MDA-MB-231 cells, knockdown of endogenous NRF1 reduced spheroid formation both in size (Fig. 2e) and number (Fig. 2f), reduced survival (Fig. 2g), induced anoikis (Fig. 2h–j), and reduced the invasive growth pattern of aggregates in Matrigel (Fig. 2k–n). Thus, NRF1 overexpression promoted spheroid formation and survival in non-tumorigenic MCF10A cells; whereas NFR1 knockdown reduced spheroid formation and survival in MDA-MB-231 breast cancer cells.

Detachment of epithelial cells from the ECM causes metabolic stress to reduce ATP, NADH, and viability [4]. One of the manifestations of detachment-induced metabolic stress is a rise in reactive oxygen species (ROS) [4]. As would be expected, ROS levels increased in detached MCF10A and MDA-MB-231 cells relative to those in attached cultures (Fig. 2o). While NRF1 did not abolish this detachment-induced ROS increase, the 10A-NRF1-OE cells showed lower ROS relative to 10A-vector (v-OE) cells in attached and detached cultures (Fig. 2o). On the other hand, NRF1 knockdown did not affect the ROS levels in attached MDA-MB-231 cells but raised ROS levels in detached culture (Fig. 2o). These results suggested that NRF1 could modulate ROS, but it was not sufficient to abrogate the ROS increase in matrix-deprived cells.

We also examined the effects of NRF1 on several regulators of metabolism including AKT, mTOR, p70-S6Kinase (p70S6K), and AMPK by assessing the levels of these kinases and their phosphorylation in attached and detached cells (Supplementary Figure S4). In MCF10A cells, NRF1 overproduction increased the levels of pAKT in attached and detached cells and that of pAMPK in detached cells (Supplementary Figure S4a and b). Increased AMPK activation has been implicated in anoikis resistance [23, 24], through inhibition of mTOR and suppression of protein synthesis [25]. In 10A-NRF1-OE detached cells, however, the higher pAMPK was associated with higher p-mTOR and p-p70S6K (Supplementary Figure S4a, c, d and e), indicating that NRF1 overproduction might support rather than inhibit metabolism in detached MCF10A cells. With MDA-MB-231 cells, NRF1 knockdown reduced p-mTOR and p-p70S6K in detached cultures (Supplementary Figure

S4a, c and d), again indicating that NRF1 contributed to the maintenance of metabolism in detached breast cancer cells.

It has been reported that $CD44^{high}/CD24^{low}$ breast cancer cells exhibit the characteristics of tumor stem cells with increased capacity to grow as spheroids in suspension cultures [8–11, 26]. We therefore examined the effects of NRF1 on the expression of CD44 and CD24 in MCF10A and MDA-MB-213 cells (Supplementary Figure 5). We found that NRF1 stimulated CD44 expression on the cell surface and at the levels of RNA, as NRF1 overexpression increased CD44 in MCF10A cells and NRF1-knockdown decreased CD44 in MDA-MB-231 cells. By contrast, NRF1 did not affect the expression of CD24 (Supplementary Figure 5a–h). We also examined the effect of NRF1 on mammary spheres derived from single cells in suspension culture by plating detached cells at low density [27], and found that NRF1 overexpression increased the number of MCF10A spheres whereas NRF1-knockdown reduced the number of MDA-MB-231 spheres (Supplementary Figure S5 i–l). These results further confirmed that NRF1 promoted the survival of matrix-deprived mammary epithelial cells.

NRF1 stimulates mitochondrial energy metabolism

NRF1 is a master regulator of nuclear genes involved in mitochondrial biogenesis and energy metabolism; [15, 16] we therefore examined the effect of NRF1 on OXPHOS by measuring the oxygen consumption rates in live cells with the Seahorse technology (Fig. 3a). In MCF10A cells, NRF1 overexpression increased the mitochondrial respiratory capacity, including the maximal respiration, the respiratory control ratio, and the spare respiratory capacity (Fig. 3c–e). The 10A-NRF1-OE cells also showed a small increase in coupling efficiency (Fig. 3f). This NRF1-induced increase in oxygen consumption was associated with higher ATP levels in attached and detached cells (Fig. 3k). We also measured the relative abundance of mitochondrial DNA (mtDNA) and found that NRF1 overexpression enhanced the mtDNA increase in detached MCF10A cells (Fig. 3m). With MDA-MB-231 breast cancer cells, NRF1 knockdown decreased mitochondrial respiratory capacity and coupling efficiency (Fig. 3b, g–j). NRF1 knockdown also reduce the levels of ATP (Fig. 3l), but had no effect on the relative abundance of mtDNA (Fig. 3n). To determine the role of OXPHOS in NRF1-stimulated spheroid survival, we treated 10A-NRF1-OE and the parental MDA-MB-231 cells with oligomycin to inhibit respiration and ATP synthesis, and found that oligomycin significantly reduced the number and the size of spheroids formed by the 10A-NRF1-OE (Fig. 3o, p) and the MDA-MB-231 cells (Fig. 3q, r). Together, results in Fig. 3 show that NRF1-stimulated OXPHOS is required for the survival of matrix-deprived MCF10A and MDAMB-231 cells.

NRF1 promotes mesenchymal traits

We noticed that 10A-NRF1-OE cells displayed spindle morphology with increased cell scattering relative to 10Avector-OE cells in attached culture (Fig. 4a). On the contrary, the typical mesenchymal phenotype of the 231-vectorKD cells was transformed to a more cobblestone-like epithelial morphology of the 231-NRF1-KD cells (Fig. 4b). To determine if these morphological changes were associated with alterations in the levels of epithelial and mesenchymal markers, we examined the effect of NRF1 on several such markers in

MCF10A, MDA-MB-231, and MCF7 cells (Fig. 4d). The stable overexpression of NRF1 in MCF7 was confirmed by qRT-PCR and immunoblotting (Fig. 4c). In MCF10A cells, NRF1 overexpression correlated with increased levels of mesenchymal markers such as CDH2 (N-cadherin), VIM (Vimentin), SNAI2 (Slug), and SNAI1 (Snail) and decreased levels of epithelial markers such as CDH1 (E-cadherin), CLDN1 (Claudin-1), and TJP1 (tight junction protein-1, ZO-1) (Fig. 4d). In MCF7 cells, NRF1 overexpression correlated with increase in VIM and decrease in CLDN1 and TJP1 (Fig. 4d). With MDA-MB231 cells, NRF1 knockdown correlated with reductions in the levels of mesenchymal markers including CDH2, VIM, SNAI2, SNAI1, and ZEB1 (Fig. 4d). These results showed a positive effect of NRF1 on the expression of mesenchymal markers and a negative one on the epithelial markers. The overexpression of NRF1 also stimulated mesenchymal traits in MCF10A cells by enhancing the rate of cell migration and invasion as demonstrated by several different assays (Fig. 5a, b, e, f, I, j). On the other hand, NRF1 knockdown reduced wound closure, migration, and invasion in MDAMB-231 breast cancer cells (Fig. 5c, d, g, h, k, l). It should be noted that NRF1 overexpression or knockdown did not affect cell proliferation in MCF10A or MDA-MB-231 cells, respectively (Fig. 5m, n). Together, results in Figs. 4 and 5 suggest that NRF1 promotes mesenchymal transition in nontumorigenic and tumorigenic mammary epithelial cells.

NRF1 promotes tumor formation and metastasis in vivo

To evaluate the effect of NRF1 on tumor growth and metastasis in vivo, we transplanted 231-vector (vKD) and 231-NRF1-shRNA (KD) cells into female nude mice (BALB/c) by orthotopic injection into the mammary fat pads or by tail–vein injection. We found that NRF1 knockdown significantly reduced tumor growth in the mammary fat pads as quantified by tumor volume and weight (Fig. 6a–c). Immunohistochemistry staining of tumor sections showed that NRF1 knockdown also reduced the expression of mesenchymal markers CDH2 and VIM (Fig. 6d). Metastasis of tumor cells from the fat pads to the lungs was detected by staining for human VIM (Fig. 6e). We found that the knockdown of NRF1 significantly reduced the metastatic burden in the lungs (Fig. 6f). Colonization of the lungs by tail-vein injected cells was also measured by histology and staining for human VIM (Fig. 6g). Again, the knockdown of NRF1 significantly reduced the number and the size of tumor colonies in the lungs of tail-vein injected mice (Fig. 6h). The reductions in tumor burden observed with the NRF1-knockdown MDAMB-231 cells provided in vivo confirmation of the in vitro findings that NRF1 promotes spheroid survival, cell migration, invasion, and epithelial to mesenchymal transition.

NRF1 expression is associated with poorer survival in luminal A subtype of breast cancer

The cell line-based results suggested that NRF1 has the potential to drive malignant progression in breast cancer. We therefore analyzed the association of NFR1 expression with survival outcome in a cohort of 632 breast cancer cases in the Gene Expression Omnibus (GEO) database. This cohort of samples allowed separation into three subgroups —ER^+/PR^+ (Luminal A), $ERBB2^+$, and triple negative (Basal-like). The Luminal B subtype was not sufficiently represented in this database for analysis. For each of the three subgroups, we divided the cases into two categories— NRF1-high (above median) and NRF1-low (below

median) and found a significant association ($P = 0.018$) of NRF1high cases with poorer survival among the Luminal A subtype of breast cancer (Fig. 7).

Discussion

Systems approach for identification of hub transcription factors from shRNA-pool screens

High throughput (NextGen) sequencing has revolutionized human genetics and enabled quantitative screen of small hairpin RNA (shRNA) or guide RNA that are enriched or depleted in pools of cells following functional selections [28–31]. Using this pool screen strategy, we identified shRNAs that were enriched in MCF10A spheroids. Following 7 rounds of selection and 98% loss of input shRNA sequences, the pool screen strategy still left us with hundreds of shRNA sequences that were too numerous to validate individually. To make sense of the pool screen results, we took a systems approach to search for TFs that the ENCODE ChIP-Seq data predict to interact with the promoter regions of the top shRNA hits. This approach, combined with a focus on the mitochondria, led us to discover a role for nuclear respiratory factor 1 (NRF1) in promoting mammary spheroid survival. Our results support this systems approach of using hits from pool-screens as nodes to construct regulatory networks for identification of master TFs that regulate the biological processes of interest. We would like to point out that this approach has deduced at least seven other transcription regulators including sequence-specific DNA binding proteins and general TFs that show higher connectivity than NRF1 to the shRNA-hits (Fig. 1f). How those other TFs contribute to the survival of mammary spheroids will wait further investigation.

Mitochondrial energy metabolism contributes to spheroid survival

It has been widely observed that epithelial cells aggregate into spheroids through cell–cell adhesion when they are deprived of cell-matrix adhesion, and this clustering can prevent anoikis. However, blocking anoikis is not sufficient for spheroid cell survival because detachment disrupts glucose metabolism and depletes ATP [4, 6]. In this study, we found that NRF1 stimulates mitochondrial energy metabolism to promote the survival of mammary spheroids in the non-tumorigenic MCF10A and the breast cancer MDA-MB-231 cells. In other words, NRF1-dependent metabolic fitness is an important factor in the survival of matrix-deprived mammary epithelial cells. Although tumor cells prefer anaerobic glycolysis as the source for energy, recent results have shown that mitochondrial respiration and metabolism remain critical to tumor growth [32–34, 18–20]. Our finding that NRF1, a master transcription regulator of energy metabolism, promotes spheroid survival by

NRF1 promotes tumor growth and metastasis

Multicellular aggregates of circulating cancer cells (CTC clusters) are potent initiators of distant organ metastasis [12]. It is therefore conceivable that increased survival of breast cancer spheroids can contribute to metastasis. We show here that NRF1 knockdown reduced MDA-MB-231 growth in the mammary fat pads and the lung tissues. Because NRF1 knockdown did not affect MDA-MB-213 proliferation in vitro, this in vivo reduction in tumor burden is likely to be associated with reductions in the survival, the migration, the invasion and the expression of mesenchymal markers of the 231-NRF1-KD cells.

Previous studies have shown that estrogen and its receptor (ER) can stimulate NRF1 expression and activity in the ER-positive MCF7 breast cancer cells [17, 35, 36]. Our analysis of one public database found an association of higher NRF1 expression with poorer survival in the Luminal A ($ER^+/PR^+/ERBB2^-$) subtype of breast cancer. Given our results that support a tumor-promoter function for NRF1, it is possible that this TF may function as a downstream mediator of the oncogenic effect of estrogen in ERpositive breast cancer.

Materials and methods

The following materials and methods are described in the Supplemental Materials and methods section:

Reagents and antibodies

Plasmids construction, viral production, and infection

Cell culture

Clonogenic survival assay

Formation of spheroid and single cell sphere

Matrigel culture

Cell viability and proliferation assay

Caspase-3 activity assay

Wound healing, Transwell migration, and Matrigel invasion assays

ATP assay

ROS assay

Measurement of mitochondrial respiration Mitochondrial DNA content measurement

RNA extraction and quantification

ChIP–quantitative real time PCR (ChIP-qPCR)

Immunoblotting

Analysis of NRF1 expression with breast cancer survival

Pooled screen of a shRNA library in MCF10A cells

A pool of genome-wide lentiviral shRNA library (SBI, SI606B-1, GeneNet Human 50 K) containing 200,000 shRNA directed against 47,400 human mRNAs was purchased from System Biosciences Company (Mountain View, CA, USA) with a titer of 1×10^7 infectious units (ifu)/ml. The detail procedures regarding shRNA library screen and sequencing of genomic shRNA integrants are described in Supplementary Methods.

Construction and analysis of shRNA hits-centered transcription factor network (sHTFN)

The UCSC Genome Browser database has collected TF ChIP-Seq dataset from ENCODE project [37], which includes binding regions of TF derived from a large collection of ChIP-Seq experiments. In this study, we defined the "promoter" as the 2-kb region upstream of the transcriptional start site and searched the ENCODE database for TF interactions in these regions. The sHTFN depicting binding interactions between the shRNA-hits and TFs was constructed using Cytoscape V3.3.0 (Fig. 2a). To determine the statistical significance of one specific TF's interactions with the group of shRNA-hits relative to its genome-wide interactions, we performed Fisher's exact test to define a *P* value, which calculates the possibility that the shRNA-hits from our screen are regulated as a cohort by one TF. In other words, this in silico analysis aimed at finding TFs whose target genes were significantly enriched in the set of 8 shRNA-hits. The formula for *P* value calculation is as follows:

$$P\text{value} = 1 - \sum_{i=0}^{m-1} \frac{\binom{M}{i}\binom{N-M}{n-i}}{\binom{N}{n}}$$

where, "*N*": total number of genes with ChIP-seq peaks in the 2 kb regions upstream of transcription start sites of all TFs for which there are ENCODE data; "*M*": number of genes with ChIP-seq peaks for a specific TF in the 2 kb regions upstream of transcription start sites; "*n*": number of shRNA-hits listed in Fig. 1d (the 8 shRNA hits with $P < 0.05$); "*m*": number of shRNA-hits with ChIP-seq peaks for a given TF in the 2 kb regions upstream of transcription start sties. The TFs with *P* value ≤ 0.05 were defined as hub TFs in the sHTFN.

Statistical analysis

Statistical significance was determined by unpaired twotailed Student's *t*-test ($P < 0.05$) and one-way ANOVA. $P < 0.05$ was considered statistically significant. The average or mean data for qRT-PCR or spheroid formation were calculated using Microsoft Excel or GraphPad Prism 5 software. For survival analysis, Kaplan–Meier curves were drawn and differences between the curves were calculated by the log-rank test using R Foundation for Statistical Computing (Vienna, Austria, 2010) software.

Supplementary Material

Refer to Web version on PubMed Central for supplementary material.

Acknowledgements

We thank J. Dai, Q. Wang, Z. Zhang, and G. Cheng for insightful comments on the study, and X. He for technical assistance. Nano-Bio-Chem Centre in Suzhou Institute of Nano-Tech and Nano-Bionics (SINANO) is acknowledged for professional assistance of cell imaging and FACS assay. This study was initiated as a pilot project in the San Diego Systems Biology Center (NIH P50GM085764) that supported G.S., D.Q., O. H., and J.Y.J.W.; D.Q. was also supported by a grant to J.Y.J.W. (NIH R01CA043054). The study of NFR1 was supported by National Natural Science Foundation of China (Grant No. 31471307), Ministry of Science and Technology (MOST) (Grant No. 2014CB965003, and 2017YFA0104301) to G.S., who is also supported by Hundred Talent Program of Chinese Academy of Sciences. The study was also supported by the CAS/SAFEA International Innovation Teams program.

References

1. Frisch SM, Francis H. Disruption of epithelial cell-matrix interactions induces apoptosis. J Cell Biol. 1994;124:619–26. [PubMed: 8106557]
2. Paoli P, Giannoni E, Chiarugi P. Anoikis molecular pathways andits role in cancer progression. Biochim Biophys Acta. 2013; 1833:3481–98 [PubMed: 23830918]
3. Vlahakis A, Debnath J. The interconnections between autophagyand integrin-mediated cell adhesion. J Mol Biol. 2017; 429:515–30. [PubMed: 27932295]
4. Schafer ZT, Grassian AR, Song L, Jiang Z, Gerhart-Hines Z, Irie HY, et al. Antioxidant and oncogene rescue of metabolic defects caused by loss of matrix attachment. Nature. 2009;461:109–13. [PubMed: 19693011]
5. Rayavarapu RR, Heiden B, Pagani N, Shaw MM, Shuff S, Zhang S, et al. The role of multicellular aggregation in the survival of ErbB2-positive breast cancer cells during extracellular matrix detachment. J Biol Chem. 2015;290:8722–33. [PubMed: 25681438]
6. Mason JA, Hagel KR, Hawk MA, Schafer ZT. Metabolism duringECM detachment: achilles heel of cancer cells. Trends Cancer. 2017;3:475–81. [PubMed: 28718402]
7. Kim YN, Koo KH, Sung JY, Yun UJ, Kim H. Anoikis resistance: an essential prerequisite for tumor metastasis. Int J Cell Biol. 2012;2012:306879. [PubMed: 22505926]
8. Dontu G, Abdallah WM, Foley JM, Jackson KW, Clarke MF,Kawamura MJ, et al. In vitro propagation and transcriptional profiling of human mammary stem/progenitor cells. Genes Dev. 2003;17:1253–70. [PubMed: 12756227]
9. Al-Hajj M, Wicha MS, Benito-Hernandez A, Morrison SJ, ClarkeMF. Prospective identification of tumorigenic breast cancer cells. Proc Natl Acad Sci USA. 2003;100:3983–8. [PubMed: 12629218]
10. Grimshaw MJ, Cooper L, Papazisis K, Coleman JA, Bohnenkamp HR, Chiapero-Stanke L, et al. Mammosphere culture of metastatic breast cancer cells enriches for tumorigenic breast cancer cells. Breast Cancer Res. 2008;10:R52. [PubMed: 18541018]
11. Dey D, Saxena M, Paranjape AN, Krishnan V, Giraddi R, Kumar MV, et al. Phenotypic and functional characterization of human mammary stem/progenitor cells in long term culture. PLoS One. 2009;4:e5329. [PubMed: 19390630]
12. Au SH, Storey BD, Moore JC, Tang Q, Chen YL, Javaid S, et al.Clusters of circulating tumor cells traverse capillary-sized vessels. Proc Natl Acad Sci USA. 2016;113:4947–52. [PubMed: 27091969]
13. Grassian AR, Schafer ZT, Brugge JS. ErbB2 stabilizes epidermalgrowth factor receptor (EGFR) expression via Erk and Sprouty2 in extracellular matrix-detached cells. J Biol Chem. 2011;286:79–90. [PubMed: 20956544]
14. Kelly DP, Scarpulla RC. Transcriptional regulatory circuits controlling mitochondrial biogenesis and function. Genes Dev. 2004;18:357–68. [PubMed: 15004004]
15. Scarpulla RC. Nuclear control of respiratory chain expression bynuclear respiratory factors and PGC-1-related coactivator. Ann N Y Acad Sci. 2008;1147:321–34. [PubMed: 19076454]
16. Scarpulla RC. Nuclear control of respiratory gene expression inmammalian cells. J Cell Biochem. 2006;97:673–83. [PubMed: 16329141]
17. Mattingly KA, Ivanova MM, Riggs KA, Wickramasinghe NS,Barch MJ, Klinge CM. Estradiol stimulates transcription of nuclear respiratory factor-1 and increases mitochondrial biogenesis. Mol Endocrinol. 2008;22:609–22. [PubMed: 18048642]
18. Tan AS, Baty JW, Dong LF, Bezawork-Geleta A, Endaya B,Goodwin J, et al. Mitochondrial genome acquisition restores respiratory function and tumorigenic potential of cancer cells without mitochondrial DNA. Cell Metab. 2015;21:81–94. [PubMed: 25565207]
19. LeBleu VS, O'Connell JT, Gonzalez Herrera KN, Wikman H, Pantel K, Haigis MC, et al. PGC-1alpha mediates mitochondrial biogenesis and oxidative phosphorylation in cancer cells to promote metastasis. Nat Cell Biol. 2014;16:992–1003. 1001–15 [PubMed: 25241037]
20. Viale A, Pettazzoni P, Lyssiotis CA, Ying H, Sanchez N, Marchesini M, et al. Oncogene ablation-resistant pancreatic cancer cells depend on mitochondrial function. Nature. 2014; 514:628–32. [PubMed: 25119024]

21. Vais H, Tanis JE, Muller M, Payne R, Mallilankaraman K, FoskettJK. MCUR1, CCDC90A, is a regulator of the mitochondrial calcium uniporter. Cell Metab. 2015;22:533–5. [PubMed: 26445506]
22. Paupe V, Prudent J, Dassa EP, Rendon OZ, Shoubridge EA.CCDC90A (MCUR1) is a cytochrome c oxidase assembly factor and not a regulator of the mitochondrial calcium uniporter. Cell Metab. 2015;21:109–16. [PubMed: 25565209]
23. Jeon SM, Chandel NS, Hay N. AMPK regulates NADPHhomeostasis to promote tumour cell survival during energy stress. Nature. 2012;485:661–5. [PubMed: 22660331]
24. Hindupur SK, Balaji SA, Saxena M, Pandey S, Sravan GS, Heda N, et al. Identification of a novel AMPK-PEA15 axis in the anoikis-resistant growth of mammary cells. Breast Cancer Res. 2014;16:420. [PubMed: 25096718]
25. Ng TL, Leprivier G, Robertson MD, Chow C, Martin MJ,Laderoute KR, et al. The AMPK stress response pathway mediates anoikis resistance through inhibition of mTOR and suppression of protein synthesis. Cell Death Differ. 2012;19:501–10. [PubMed: 21941369]
26. Mani SA, Guo W, Liao MJ, Eaton EN, Ayyanan A, Zhou AY,et al. The epithelial-mesenchymal transition generates cells with properties of stem cells. Cell. 2008;133:704–15. [PubMed: 18485877]
27. Qu Y, Han B, Yu Y, Yao W, Bose S, Karlan BY, et al. Evaluationof MCF10A as a reliable model for normal human mammary epithelial cells. PLoS One. 2015;10:e0131285. [PubMed: 26147507]
28. Oliver D, Ji H, Liu P, Gasparian A, Gardiner E, Lee S, et al.Identification of novel cancer therapeutic targets using a designed and pooled shRNA library screen. Sci Rep. 2017;7:43023. [PubMed: 28223711]
29. Sims D, Mendes-Pereira AM, Frankum J, Burgess D, Cerone MA,Lombardelli C, et al. High-throughput RNA interference screening using pooled shRNA libraries and next generation sequencing. Genome Biol. 2011;12:R104. [PubMed: 22018332]
30. Koike-Yusa H, Li Y, Tan EP, Velasco-Herrera Mdel C, Yusa K.Genome-wide recessive genetic screening in mammalian cells with a lentiviral CRISPR-guide RNA library. Nat Biotechnol. 2014;32:267–73. [PubMed: 24535568]
31. Zhou Y, Zhu S, Cai C, Yuan P, Li C, Huang Y, et al. Highthroughput screening of a CRISPR/Cas9 library for functional genomics in human cells. Nature. 2014;509:487–91. [PubMed: 24717434]
32. Dey P, Baddour J, Muller F, Wu CC, Wang H, Liao WT, et al. Genomic deletion of malic enzyme 2 confers collateral lethality in pancreatic cancer. Nature. 2017;542:119–23. [PubMed: 28099419]
33. Sullivan LB, Gui DY, Hosios AM, Bush LN, Freinkman E,Vander Heiden MG. Supporting aspartate biosynthesis is an essential function of respiration in proliferating cells. Cell. 2015;162:552–63. [PubMed: 26232225]
34. Birsoy K, Wang T, Chen WW, Freinkman E, Abu-Remaileh M,Sabatini DM. An essential role of the mitochondrial electron transport chain in cell proliferation is to enable aspartate synthesis. Cell. 2015;162:540–51. [PubMed: 26232224]
35. Ivanova MM, Luken KH, Zimmer AS, Lenzo FL, Smith RJ, Arteel MW, et al. Tamoxifen increases nuclear respiratory factor 1 transcription by activating estrogen receptor beta and AP-1 recruitment to adjacent promoter binding sites. FASEB J. 2011;25:1402–16. [PubMed: 21233487]
36. Mattingly KA, Klinge CM. Diesel exhaust particulate extractsinhibit transcription of nuclear respiratory factor-1 and cell viability in human umbilical vein endothelial cells. Arch Toxicol. 2012;86:633–42. [PubMed: 22105178]
37. Rosenbloom KR, Sloan CA, Malladi VS, Dreszer TR, Learned K,Kirkup VM, et al. ENCODE data in the UCSC Genome Browser: year 5 update. Nucleic Acids Res. 2013;41:D56–63. [PubMed: 23193274]

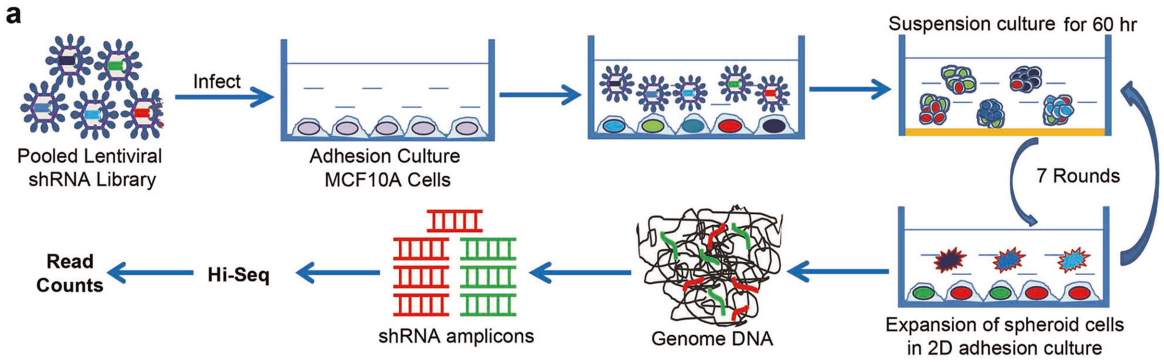

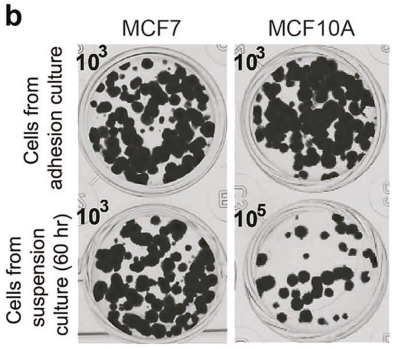

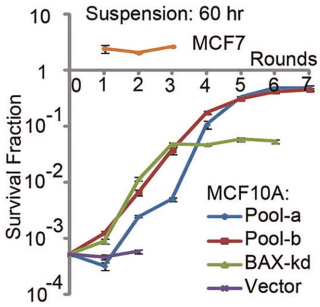

d

Top eight shRNA Hits

shRNA Hits	Fold Enrichment in spheroids	P value (Binomial)
CCDC90B	91.3	0.0000
IDH3B	22.9	0.0205
IL13RA1	10.8	0.0200
AJAP1	10.2	0.0104
LITAF	7.6	0.0104
PUDP	7.6	0.0104
LRP12	5.1	0.0205
GEMIN2	4.1	0.0497

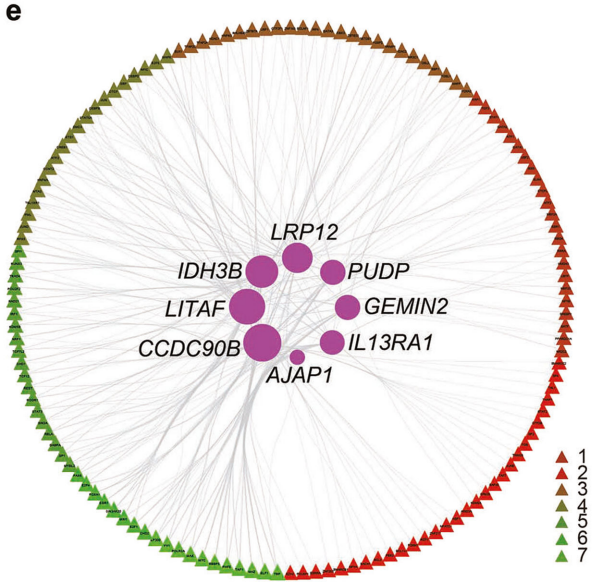

f

TFs	Degree Rank	Degree	P-value
PHF8	1	7	3.23E-03
RBBP5	1	7	4.62E-03
ELF1	1	7	9.62E-03
MAZ	1	7	1.12E-02
TAF1	1	7	1.17E-02
TBP	1	7	1.21E-02
YY1	1	7	1.65E-02
NRF1	**3**	**5**	**1.80E-02**
E2F4	2	6	1.96E-02
MAX	1	7	2.15E-02
E2F1	2	6	2.32E-02
MYC	1	7	2.36E-02
EP300	1	7	2.58E-02
PAX5	2	6	2.80E-02
POLR2A	1	7	3.14E-02
MYBL2	3	5	4.28E-02
CHD2	2	6	4.28E-02

Fig. 1.

Identification of NRF1 as a transcription factor with significant connectivity to shRNA-hits from MCF10A cells selected for clonogenic survival in spheroids. **a** Schematic summary of shRNA library pool screen strategy. **b** Representative images of clonogenic survival assay. The indicated number of MCF10A or MCF7 cells from attached or suspension cultures (60 h) were seeded and colonies stained with crystal violet at 8 days after seeding. **c** Survival rates (colony numbers/ cells seeded) of MCF10A pools transduced with shRNA-vector (violet), shRNA library screen in two independent experiments, Pool-a (blue), Pool-b (red),

and those knocked-down for BAX (BAX-kd) (green), as well as MCF7 cells (orange) after each round of suspension culture as spheroids. Error bars represent S.D. from the average value ($n = 3$). **d** The predicted gene hits of enriched shRNA sequences. **e** The visualized sHTFN reflecting regulatory relations between shRNA hits and transcription factors (TFs). The triangle nodes represent TFs predicted to bind the promoters (2000 bp upstream of the transcription start site) of the 8 shRNA hits based on the ChIP-Seq dataset from ENCODE, with the degree ranking shown in color from red (high) to green (low). Circular nodes (purple) represent the top 8 shRNA hits with the size of each circle corresponding to different number of links to TFs. **f** The topological properties of hub TFs with p value < 0.05. *NRF1* is highlighted in red. “Degree” is the number of edges connecting each TF to the top 8 shRNA hits. “Degree Rank” is the rank of each TF by the number of connecting edges, e.g., rank 1 indicates connection to all 8 shRNA-hits

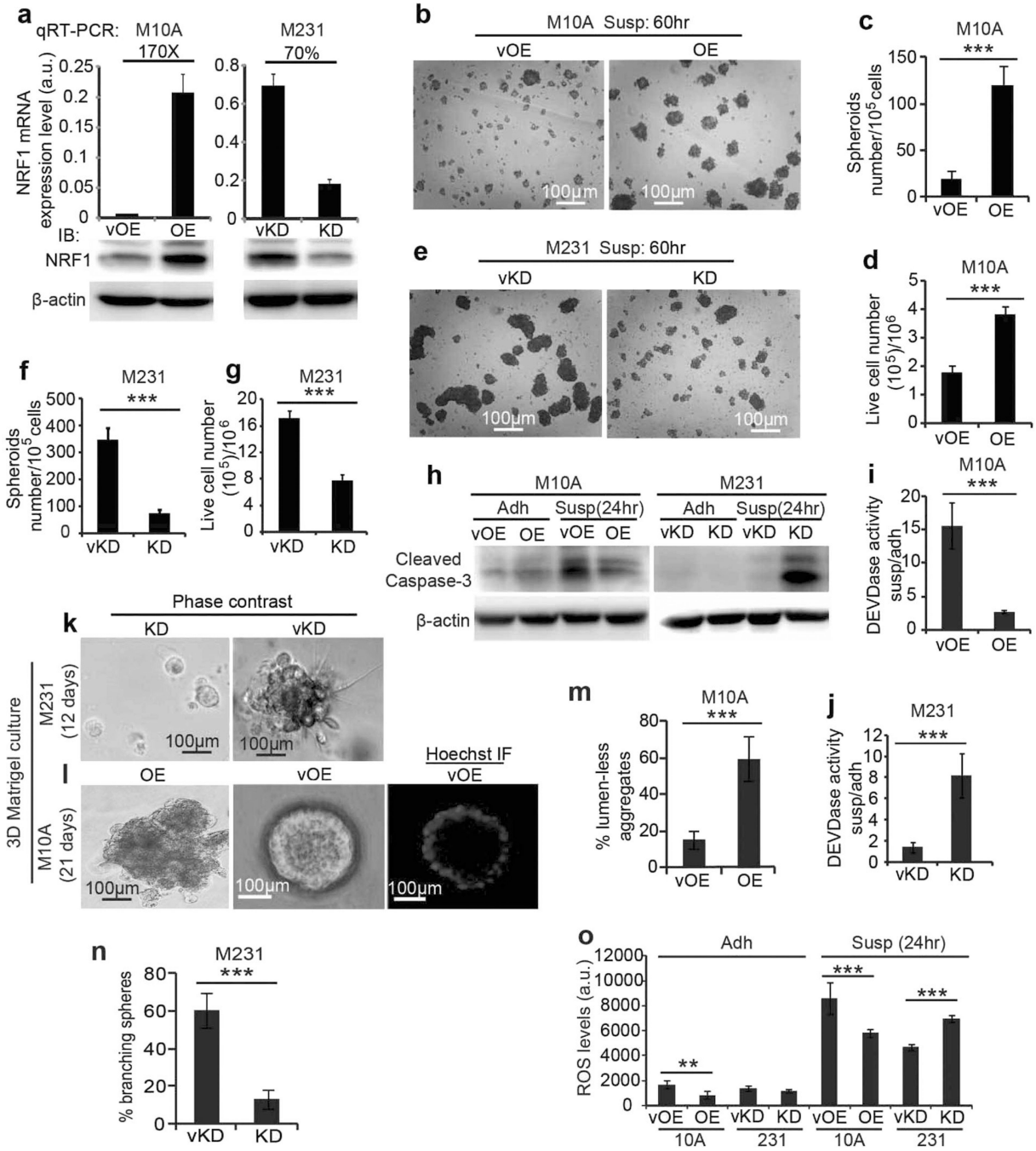

Fig. 2.

NRF1 promotes spheroid survival. **a** NRF1 overexpression in MCF10A cells (OE) and NRF1 knockdown in MDA-MB-231 cells (KD) cells determined by Western blotting and qRT-PCR. “OE” 10ANRF1-OE, “vOE” 10A-vector-OE, MCF10A vector control for OE, “KD” 231-NRF1-KD, “vKD” 231-vector-KD, MDA-MB-231 vector control for KD. **b** Representative images of spheroids of 10A-NRF1OE cells (OE) and vector control cells 10A-vector-OE (vOE) cultured in suspension for 60 h. Scale bar = 100 μm. The number of spheroids larger than 50 μm in diameter was counted and the values were shown in **c. d** Live

cells remaining after 60 h suspension culture were counted by trypan blue exclusion. **e** Representative images of spheroids of 231NRF1-KD (KD) and vector control cells 231-vector-KD (vKD) cultured in suspension for 60 h. Scale bar = 100 μm. The number of MDA-MB-231spheroids larger than 80 μm in diameter were counted and showed in **f**. **g** Live MDA-MB-231cells remaining after 60 h suspension culture were counted by trypan blue exclusion. **h** Levels of cleaved caspase-3 in lysates of the indicated cells after 24 h of suspension culture. Beta-actin was processed in parallel as an internal control for protein loading. **i, j** Fold increase in DEVDase activity in the indicated cells after 24 h suspension cultures relative to detached cultures. Representative bright field or confocal images of Matrigel culture of (**k**) the indicated MCF10A cells and (**l**) the indicated MDAMB-231 cells. Scale bar = 50 μm. The percentage of (**m**) lumen-less aggregates of MCF10A and (**n**) branching tumor spheres of MDAMB-231 cells was counted from 4 independent experiments. **o** Levels of reactive oxygen species (ROS) in the indicated cells (adhesion or suspension culture for 24 h). Data shown are mean and S.D. from three independent experiments. $^{**}P < 0.01$; $^{***}P < 0.005$, P values were determined using a two-tailed Student's t-test; a.u. arbitrary unit, Adh adhesion culture, Susp suspension culture, "M10A" and "M231" MCF10A and MDA-MB-231 cells, respectively

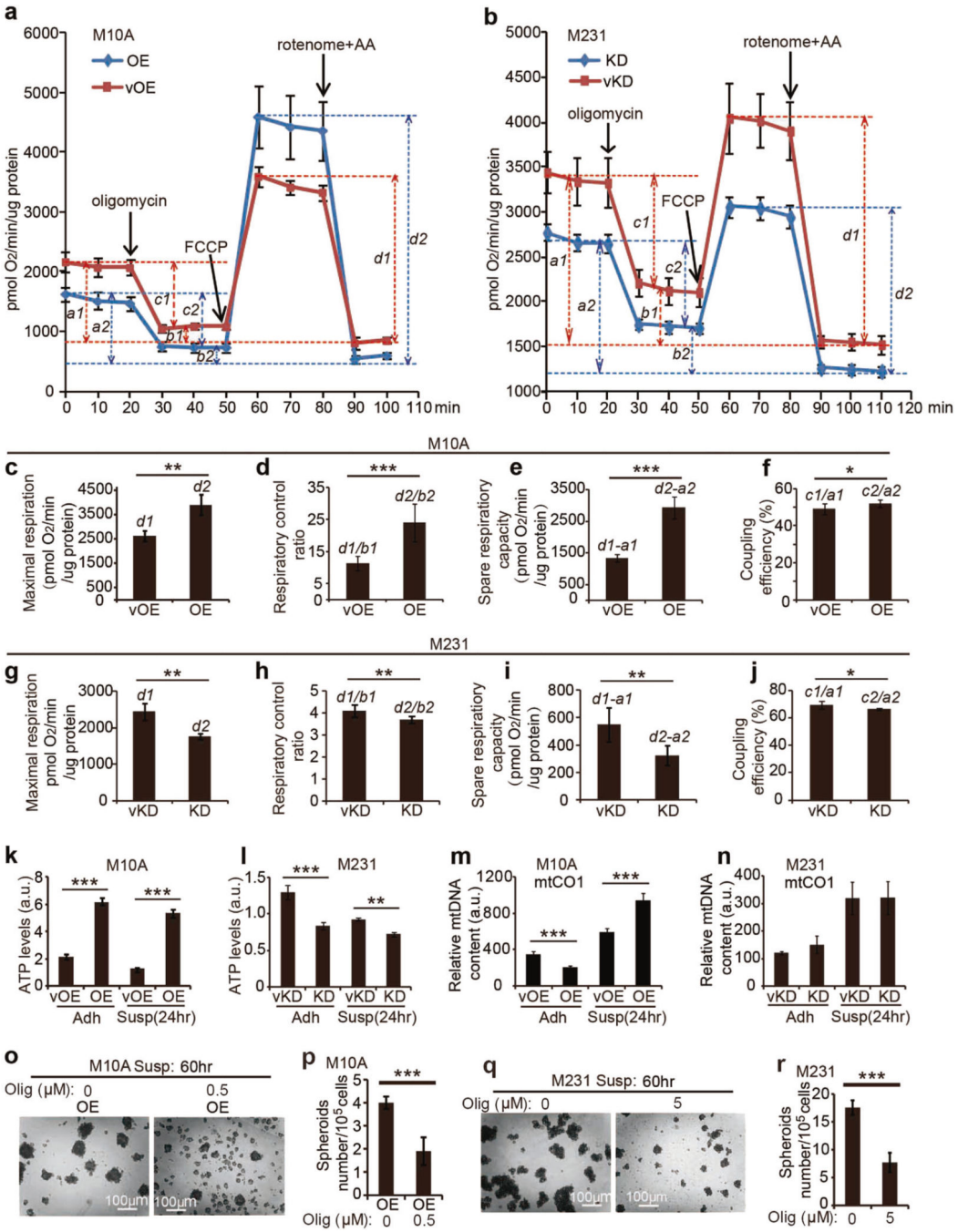

Fig. 3.

NRF1 stimulates mitochondrial respiratory capacity. **a, b** Relative oxygen consumption rate (OCR) normalized to protein content in (**a**) 10A-NRF1-OE (OE) or (**b**) 231-NRF1-KD (KD) cells. N = 3; *a1* and *a2*: basal respiration; *b1* and *b2*: oligomycin-insensitive respiration; *c1* and *c2*: oligomycin-sensitive respiration; *d1* and *d2*: maximal respiration. Accordingly, the values of maximal respiration (*d1* and *d2*), respiratory control ratio (*d1/b1* and *d2/b2*), spare respiratory capacity (*d1-a1* and *d2-a2*) and coupling efficiency (*c1/a1* and *c2/a2*) for MCF10A derived cells are shown in **c–f**, respectively; those values for MDA-MB-231

derived cells are shown in **g–j**, respectively. ATP levels of (**k**) MCF10A derived cells and (**l**) MDAMB-231 derived cells subjected to 24 h of suspension culture. Relative mitochondrial DNA (mtDNA) content of (**m**) MCF10A derived cells and (**n**) MDA-MB-231 derived cells subjected to 24 h of suspension culture. **o** Representative images of spheroids of 10A-NRF1-OE cells (OE) treated with 0.5 μm oligomycin. Scale bar = 100 μm. The number of spheroids larger than 50 μm in diameter was counted and the values were shown in **p**. **q** Representative images of spheroids of M231 cells treated with 5 μm oligomycin. Scale bar = 100 μm. The number of spheroids larger than 80 μm in diameter was counted and the values were shown in **r**. *$P < 0.05$, **$P < 0.01$, ***$P < 0.005$, P values were determined using a two-tailed Student's t-test; error bars represent S.D. from average value of three biological replicates; "Adh" adhesion culture, "Susp" suspension culture, "a.u." arbitrary unit, "OE" 10A-NRF1-OE, "vOE" 10A-vector-OE, MCF10A vector control, "KD" 231-NRF1-KD, "vKD" 231-vector-KD, MDA-MB-231 vector control; "M10A" and "M231" MCF10A and MDA-MB-231 cells, respectively, "Olig" oligomycin

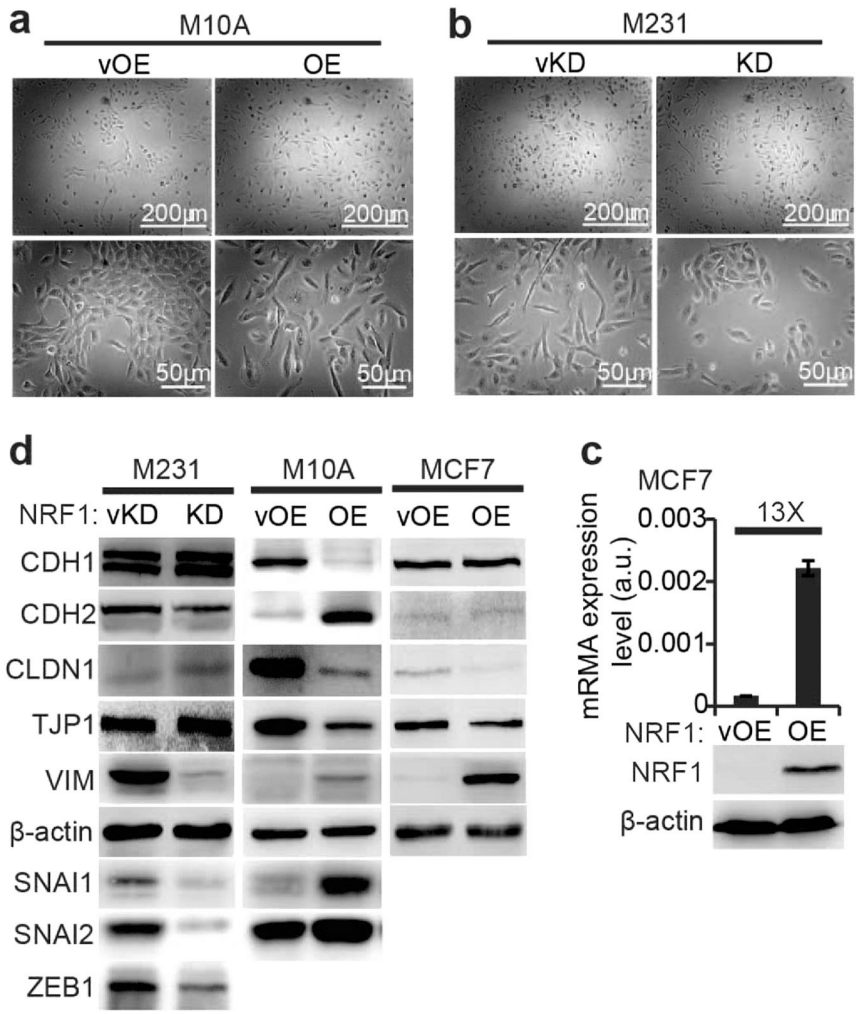

Fig. 4.

NRF1 promotes and maintains mesenchymal traits. **a** Morphology of MCF10A derived cells and **b** MDA-MB231 derived cells in adhesion culture. Scale bars are 200 μm in upper and 50 μm in lower images. **c** NRF1 overexpression in MCF7 cells (OE) cells determined by Western blotting and qRT-PCR; here, “OE” MCF7-NRF1-OE, “vOE” MCF7-vector-OE. **d** Immunoblotting assay of epithelial and mesenchymal markers in MCF10A (M10A), MDA-MB-231 (M231) and MCF7 derived cells. “OE” NRF1 overexpression, “vOE” vector control for “OE”, “KD” 231-NRF1-KD, “vKD” 231vector-KD, MDA-MB-231 vector control, “M10A” and “M231” MCF10A and MDA-MB-231 cells, respectively; “a. u.” arbitrary unit

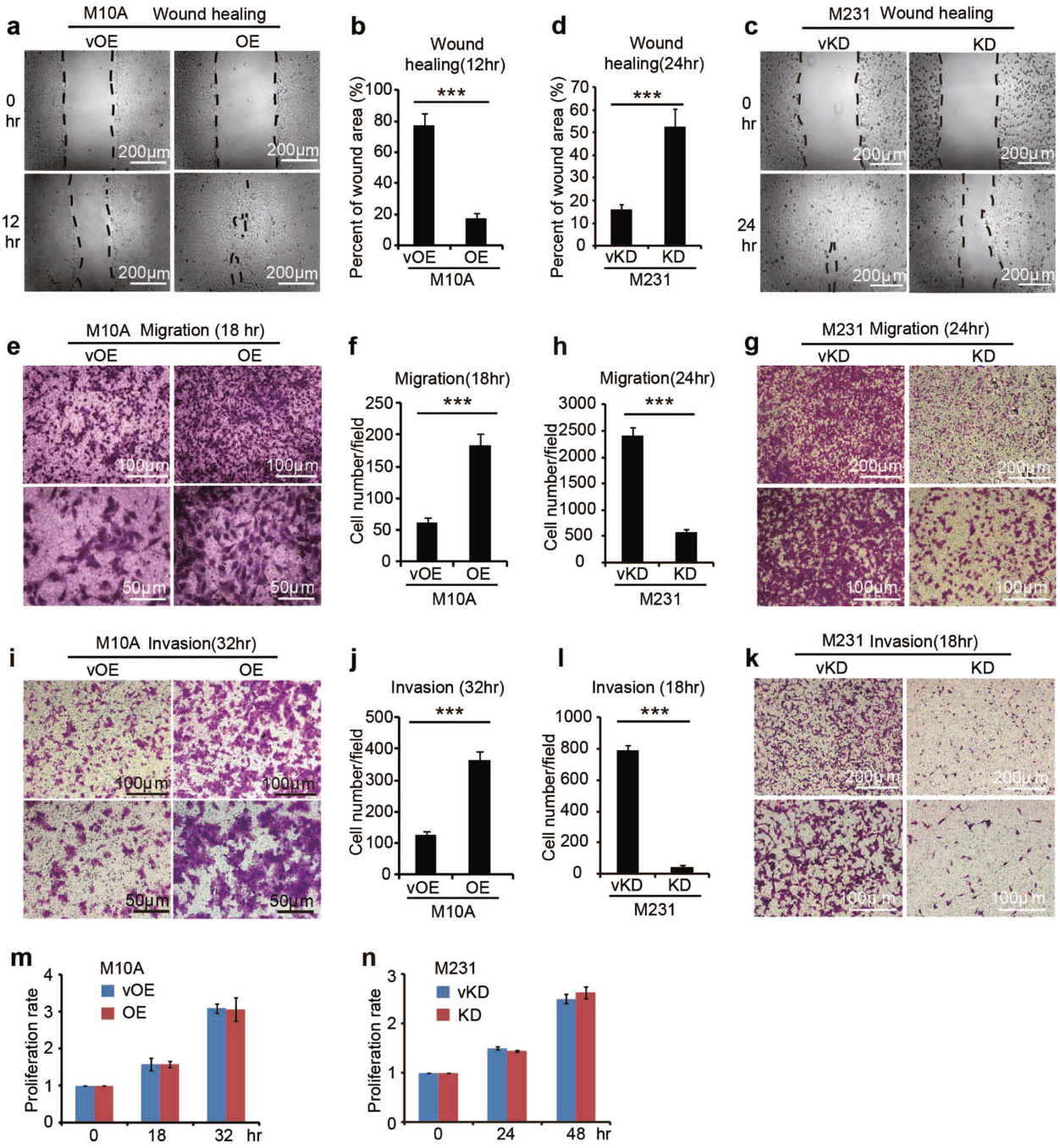

Fig. 5.

NRF1 promotes cell migration and invasion. **a, b** Wound healing assays of MCF10A derived cells and **c, d** MDA-MB-231 derived cells. Representative images were captured at indicated time of wounding (**a, c**). Dashed line represents the wound edge. Scale bar = 200 μm. **b, d** Percentage of wound healing at indicated time points. **e, f** Transwell migration assays of MCF10A derived cells and **g, h** MDA-MB-231 derived cells. Representative images were captured at indicated time of cell culture (**e, g**). Scale bars are shown in the images. The number of migrated cells in each visual field was counted (**f**, **h**). **i, j** Invasion assays of

MCF10A derived cells and **k**, **l** MDAMB-231 derived cells. Representative images were captured at indicated time of cell culture (**i**, **k**). Scale bars are shown in the images. The number of invasive cells in each visual field was counted (**j**, **l**). **m** The proliferation of MCF10A derived cells and **n** MDA-MB-231 derived cells at indicated time points. All experiments were repeated at least thrice. ***$P < 0.005$, P values were determined using a twotailed Student's *t*-test; error bars represent S.D. from average value of three biological replicates; "OE" 10A-NRF1-OE, "vOE" 10A-vectorOE, MCF10A vector control, "KD" 231-NRF1-KD, "vKD" 231vector-KD, MDA-MB-231 vector control; "M10A" and "M231": MCF10A and MDA-MB-231 cells, respectively stimulating OXPHOS, supports the emerging concept that mitochondria plays an important role in tumor development.

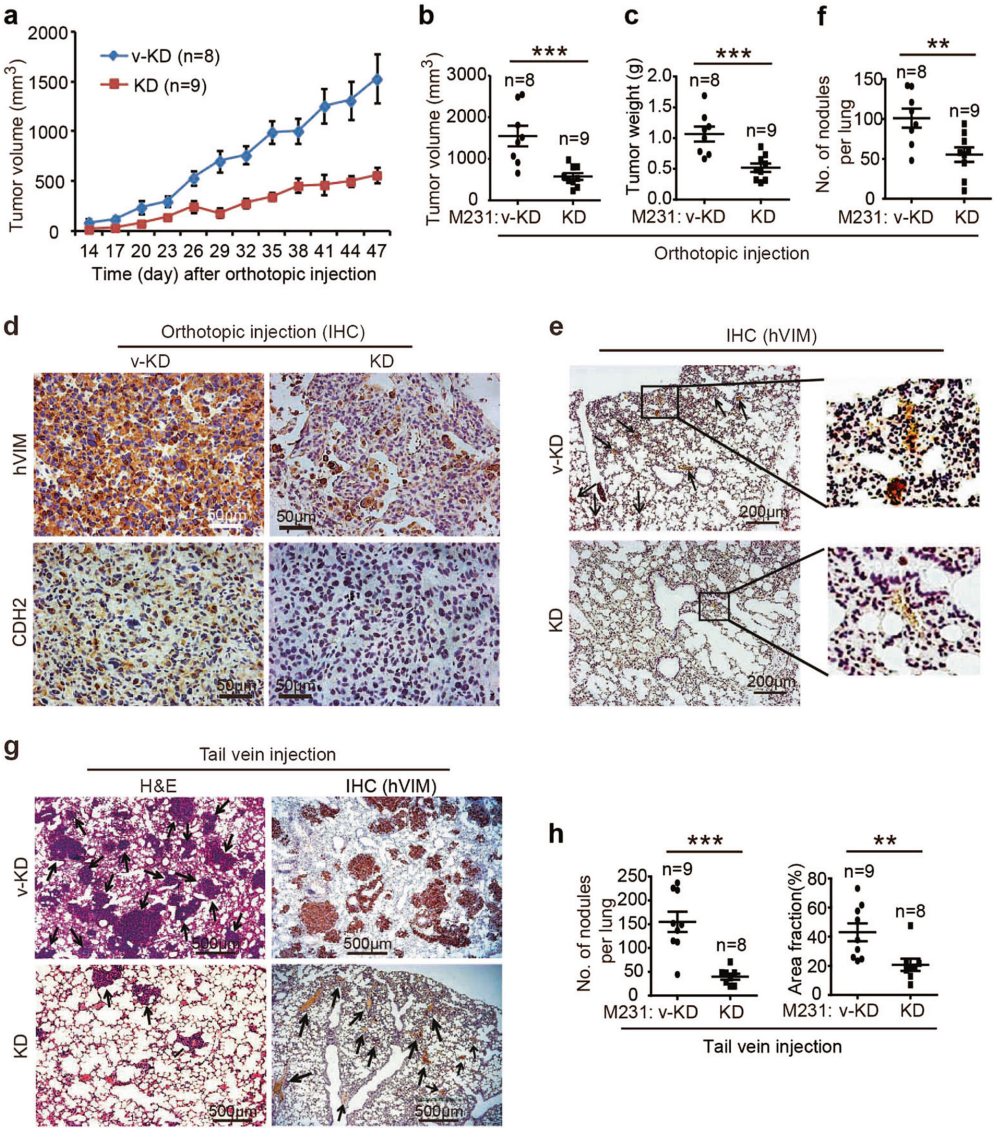

Fig. 6.

NRF1 knockdown reduces MDA-MB-231 growth in mammary fat pads and lung tissues Orthotopic injection: 231-NRF1-KD (KD) and vector control (231-vector-KD, vKD) cells were injected into the mammary fat pads (6×10^6 cells per pad) of immunodeficient mice. **a** The tumor volumes were measured at the indicated days **b** tumor volumes measured at day-47 in euthanized mice **c** tumor weights measured at day-47. **d** Immunohistochemistry (IHC) staining for hVIM and CDH2 in tumor sections **e** IHC staining for hVIM in lung tissue sections **f** number of hVIM-positive nodules in the lungs of mice from orthotopic injections. Tail vein injection: 231-NRF1-KD (KD) and vector control (231-vector-KD, vKD) cells were injected into immunodeficient mice through the tail veins (1×10^6 cells/per mouse) and the mice were killed after 42 days. **g** H&E and IHC (hVIM) staining of lung tissue sections; h the number and size of metastatic nodules. $^{**}P < 0.01$, $^{***}P < 0.005$, P values were determined using a two-tailed Student's t-test; results are expressed as mean ± SD from the indicated number of mice

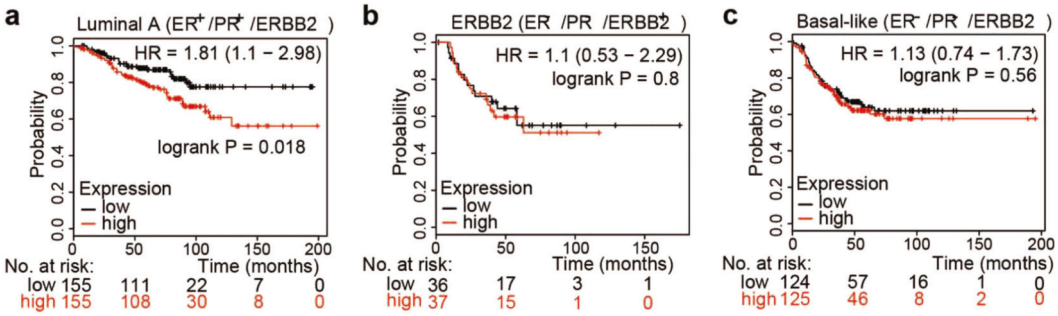

Fig. 7.

Association of NRF1 expression with survival in breast cancer subtypes. (**a–c**) Kaplan–Meir survival analysis of breast cancer stratified for three subtypes (Luminal A, ERBB2 and Basal-like) with the number of patients in each cohort: 310, 73, and 249, respectively. The black curve represents samples with below-mean expression of NRF1 (low); red curve represents samples with above-mean expression of NRF1 (high). *HR* hazard ratio